



# Preparation of Ag@SiO<sub>2</sub> core–shell nanoparticles for plasmonic dye-sensitized solar cell application using laser ablation in liquid technique

Mohammed Adil Mohammed<sup>1</sup> · Odai N. Salman<sup>2</sup> · Mehmet Mahir Bülbül<sup>1</sup>

Received: 5 September 2023 / Accepted: 20 October 2023 / Published online: 23 November 2023  
© The Author(s), under exclusive licence to Springer Science+Business Media, LLC, part of Springer Nature 2023

## Abstract

In this work, Ag@SiO<sub>2</sub> core–shell nanoparticles were prepared using the laser ablation technique and employed these nanoparticles in plasmonic-sensitized solar cells (DSSC). Current–voltage (I–V) characteristic curves of DSSCs were performed both in the dark and under 100 mW/cm<sub>2</sub> and obtained experimental results compared to each other at room temperature. Ag@SiO<sub>2</sub> core–shell NPs were prepared using different laser energies (50 mJ, 100 mJ, 150 mJ) by pulsed laser ablation in an aqueous silica solution. The results highly showed the effect of the used laser energy on the structural properties of the prepared nanoparticles, which in turn affect the other properties. The XRD for Ag@SiO<sub>2</sub> shows that the crystallinity enhanced, and the crystallite size increased with increasing the laser energy (18.8 nm for 50 mJ, 24.5 nm for 100 mJ, 34.9 nm for 150 mJ). The transmission electron microscopy shows an increasing average diameter for both NPs types with the laser energy. The UV–visible absorbance shows significant plasmonic resonance bands around 400 nm for the Ag@SiO<sub>2</sub>, with a small red shift increasing the laser energy. Incorporating metal NPs into solar cell layers enhances their efficiency by increasing the active layer's absorption, especially at the plasmonic frequency. The effect of the different NPs was examined and compared with the bare-solar cell without nanoparticles. The DSSC solar cell composed of Ag@SiO<sub>2</sub> NPs significantly enhances their characteristics. The results revealed that Ag@SiO<sub>2</sub> could be employed as selective scattering factors, promising efficient DSSCs.

**Keywords** Core–shell · Nanostructure · Laser ablation · Plasmon · Dye-sensitized solar cells

✉ Mohammed Adil Mohammed  
Ndt.casper@gmail.com

Odai N. Salman  
Odai.n.salman@uotechnology.edu.iq

Mehmet Mahir Bülbül  
mahir@gazi.edu.tr

<sup>1</sup> Faculty of Science Department of Physics, Gazi University, Ankara, Turkey

<sup>2</sup> Department of Applied Sciences, University of Technology, Baghdad, Iraq

## 1 Introduction

In a solar cell that uses dye sensitization, photon-absorbing dye molecules are loaded by nanospheres or microspheres made of semiconductor material with a wide band gap. Examples of such materials are titanium dioxide and zinc dioxide. These oxide films not only function as a semiconducting medium but also as a medium for the diffusion of electrons generated by light (O'Regan and Grätzel 1991; Choudhury 2020; Baby et al. 2022; Arka et al. 2021; Yang et al. 2022). Following the charge separation process, transporting carriers to the charge collector via the semiconductor's conduction band happens due to photon-induced electron injection from excited dye molecules into the semiconductor's conduction band. Therefore, the total efficiency of a DSSC relies greatly on the surface area and pore widths of the semiconductors used in the device. One of the defining features of a DSSC is its near-perfect efficiency in converting incident photons into electric current from the ultraviolet/visible to the near-infrared region of the electromagnetic radiation spectrum.

Consequently, the present generation of solar cells can provide a feasible supply of clean energy at a reasonable cost (Maka and Alabid 2022; Salman et al. 2023; Sampaio et al. 2017; Furugori et al. 2017; Eicke et al. 2022; Mehmood et al. 2015). The research that's been done on this topic has uncovered several different ways that DSSCs can be made more effective. Increasing the thickness of the semiconductor film is one example. Other instances include modifying the shape and size of semiconductor material on the nano- and micro-scale and altering the structural makeup of dye molecules to achieve a better spectrum response (Arinze et al. 2016; Rahman et al. 2023; Agrawal et al. 2022; Noorasid et al. 2022; Alkuam et al. 2018; Dragonetti et al. 2018; Huang et al. 2018; Park et al. 2019; Drexhage 1970).

An increase in the thickness of the semiconductor film makes it possible to load a greater quantity of dye; however, this also increases the diffusion path length for photogenerated electrons. Additionally, thicker films have a greater propensity to contain structural flaws, which increases the amount of electron trapping (Mehmood et al. 2015; Arinze et al. 2016; Rahman et al. 2023; Agrawal et al. 2022; Noorasid et al. 2022). A cutting-edge strategy for improving thin-film solar cell systems is using plasmonic metal nanoparticles, such as gold or silver. This effect has improved the efficiency of thin-film inorganic, organic, and DSSCs. Nanoparticles made of noble metals like gold and silver can boost an optical field because of a property of light called Localized surface plasmon resonance (LSPR) (Arinze et al. 2016; Mandal 2022; Selvapriya et al. 2022; Di and Qin 2022; Yen et al. 2017; Septiningrum et al. 2022; Kankanamge et al. 2023; Salimi et al. 2019; Bao et al. 2019; Fallah et al. 2019).

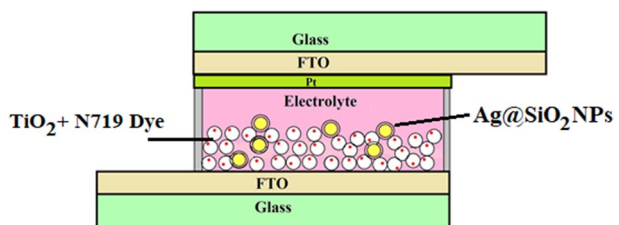
When the surface electrons of a metal nanoparticle collectively move, plasmons are created, which can increase the intensity of the electromagnetic field adjacent to the nanoparticle's surface. Nearby fluorophores may experience enhanced light extinction due to the LSPR phenomenon (Zhang et al. 2016; Kaimuangpak et al. 2023; Juma et al. 2023; Akram et al. 2023; Bhojanaa et al. 2023). Several specific applications of the LSPR phenomena have been established. Solar cells can improve their light absorption through various important methods: Dipole–dipole pairing, light scattering, and localized near-field pairing energy transfer (Bao et al. 2019). LSPR assist as a trap for light due to interaction between the confined charge within the particle with the incoming light, which causes a scattering effect (Villanueva-Cab et al. 2018). By creating a large electromagnetic field on the metal NP's surface and increasing the dye's absorption force in the visible range of

wavelengths, LSPR can increase the solar conversion efficiency ( $\eta$ ) of DSSCs (Villanueva-Cab et al. 2018). Increased light absorption caused by the LSPR effect, a negative shift in the Fermi energy level due to the electron storage effect, a rapid injection of electrons into semiconductor materials, and accelerated charge separation as a result of a localized electromagnetic field are all effects of the incorporation of metallic nanoparticles into photoanodes (Alkhalayfeh et al. 2021). The two main categories of light-trapping techniques are decreasing the top surface's reflection coefficient and lengthening the optical path inside the cell. A rise in absorption causes a decline in the recombination rate, an increase in open circuit voltage, and a rise in conversion efficiency (He et al. 2020; Rho et al. 2018; Guo et al. 2018). Bi et al. (2020) studied the DSSC and LSPR for efficient perovskite solar cells using infrared to the visible conversion of the nanoparticle to the plasmonic solar cell. They provide a successful technique for boosting luminous quantum yield. Ali et al. (2019) studied the light-harvesting process using plasmonic AuNPs to enhance light absorption in dye-sensitized solar cells. The outcomes demonstrated an increase in power conversion efficiency. Compared with the reference cell. Different parameters affect the characterization of prepared nanoparticles by PLA, consisting of the used liquid, laser energy, laser duration, etc. In this work, Ag@SiO<sub>2</sub> NPs were prepared in laser ablation technique by Nd-YAG pulsed laser at different laser energies. Then, a comparison was made between the prepared core-shell nanoparticles with different energies (50 mJ, 100 mJ, 150 mJ), and the effect of the energy difference on the dimension of the prepared core-shell (nanoparticles) was seen through XRD, PL, and UV-vis results. Researching how plasmon affects dye-sensitized solar cells, these cells were made with and without the produced core-shell nanoparticles.

## 2 Material and method

Pulse Laser Ablation in Liquid was used to create Ag@SiO<sub>2</sub> NPs. A 9 ns-pulsed Nd:YAG laser (World health care solution, 9 ns pulse duration, 1064 nm, 10 Hz, laser fluence of 17–50 J cm<sup>-2</sup>) was focused onto a silver target (ounces, purity 999.9%) immersed in 20 ml distilled water containing 0.4  $\mu$ M NaCl (AVONCHEM, purity 99.5%) and 0.4  $\mu$ M NaSiO<sub>2</sub> (sodium silicate), the procedure took 1 min to complete. To separate the Ag@SiO<sub>2</sub> Nanoparticles from the residual sodium-water glass, they were centrifuged for 10 min at 5000 rpm. The Ag@SiO<sub>2</sub> film was formed on a glass substrate using the droop casting process for XRD investigation. The absorption and PL spectra were obtained using a Shimadzu UV-1900i UV-Vis Spectrophotometer and a Varian CARY ECLIPSE. The samples were examined using a transmission electron microscopy (TEM) microscope (ZEISS LEO 912AB/Germany). Ag@SiO<sub>2</sub> NPs was loaded to DSSC as shown in Fig. 1. Regular and Plasmonic DSSC I-V measurements were made using a (Keithley 2400) Solar Simulator in the dark and under 100 mW/cm<sup>2</sup> light intensity at room temperature.

**Fig. 1** Schematic diagram of plasmonic DSSC

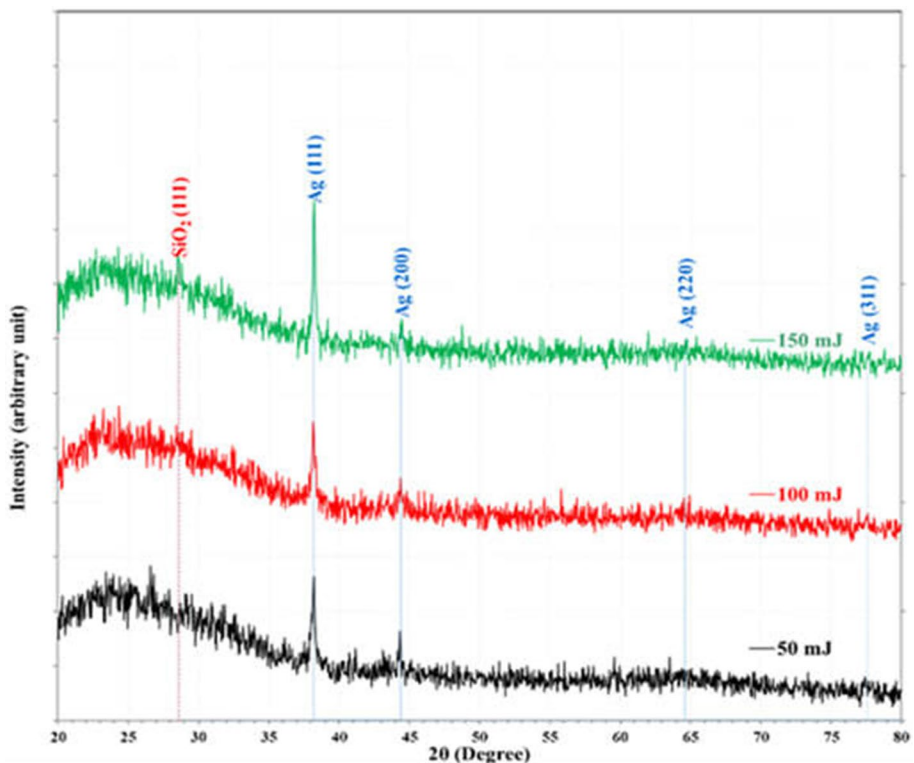


### 3 Results and discussions

Formation of Silver nanoparticles by laser ablation technique was confirmed by XRD spectrum (Fig. 2) peaks (111) and (200) pointing out the FCC phase of silver nanoparticles (Crystallography open database (COD) 9012431). The peak broadening in the XRD pattern indicates that small nanocrystals exist in the samples.

The lattice constants  $a=b=c=4.0785$ ,  $4.0800$  and  $4.0816$  Å for laser energies 50, 100, and 150 mJ, respectively, calculated from XRD data and using equation (1) (Ali et al. 2019). Table 1 illustrates the XRD results, matching the interplanar spacing (dhkl) with the COD data card and matching (h k l) planes. The Scherrer formula equation was used to estimate the crystallite size of nanocrystals Eq. (2) (Salman and Ismail 2014). Using the Stokes and Wilson Eq. (3), we can determine how much micro strain contributes to the overall line widening of the diffraction peak (Rong et al. 2019). Figure 3 shows the crystallite size as a function of laser energy for Ag@SiO<sub>2</sub> NPs. It is clear that when the laser energy increases, the crystallite size increases.

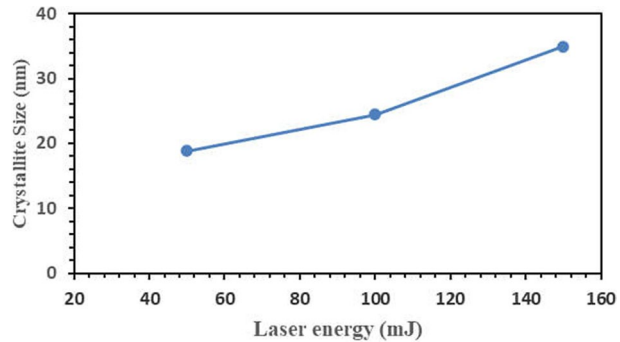
$$d = \frac{a}{\sqrt{h^2 + k^2 + l^2}} \quad (1)$$



**Fig. 2** XRD pattern of Ag@SiO<sub>2</sub> core-shell nanoparticles prepared by laser ablation technique (black lines 50 mJ, red lines 100 mJ, and green lines 150 mJ)

**Table 1** Summarizes the results of the XRD measurement

Laser energy (mJ)	2θ (°)	FWHM (°)	d <sub>hkl</sub> Exp. (Å)	C.S (nm)	d <sub>hkl</sub> Std. (Å)	Phase	hkl
50	38.1891	0.4470	2.3547	18.8	2.3543	Cub. Ag	(111)
	44.3895	0.4813	2.0391	17.8	2.0389	Cub. Ag	(200)
100	38.1747	0.3438	2.3556	24.5	2.3543	Cub. Ag	(111)
	44.3638	0.3439	2.0403	24.9	2.0389	Cub. Ag	(200)
150	28.5272	0.4470	3.1264	18.3	2.3543	Orth.SiO <sub>2</sub>	(111)
	38.1591	0.2407	2.3565	34.9	2.3543	Cub. Ag	(111)
	44.3570	0.3094	2.0406	27.7	2.0389	Cub. Ag	(200)

**Fig. 3** Crystallite size versus laser energy for Ag@SiO<sub>2</sub> NPs**Table 2** Summarizes the results of some XRD calculations for the (111) plane

Laser energy (mJ)	a (Å)	CS (nm)	Microstrain
50	4.0785	18.8	0.0018
100	4.0800	24.5	0.0014
150	4.0816	34.9	0.0010

If we use Bragg's equation to calculate the distance between crystal planes, we get  $d$ , where  $a$  is the lattice constant, and  $hkl$  is the Miller plane.

$$\text{Crystallite size}(C \cdot s) = \frac{K\lambda}{\beta \cos \theta} \quad (2)$$

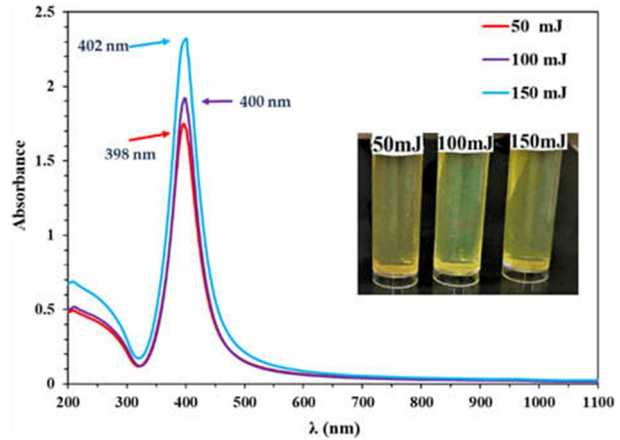
Shape factor  $k$ , X-ray incident wavelength  $\lambda$ , peak full width at half-maximum (FWHM) in radians  $\beta$ , and Bragg angle  $\Theta$ .

$$\beta_\epsilon = 4\epsilon \tan \theta \quad (3)$$

where ( $\epsilon$ ) represents the microstrain (Table 2).

Absorption spectra of Ag@SiO<sub>2</sub> nanoparticle samples generated by pulsed laser ablation at varying pulse laser energy are displayed in Fig. 4. Depending on the particle size, shape, aggregation state, and surrounding dielectric medium, the SPR causes a red or blue shift in

**Fig. 4** Absorbance relates to the wavelength of Ag@SiO<sub>2</sub> core-shell nanoparticles for different laser energies. The inset shows the images of Ag@SiO<sub>2</sub> samples



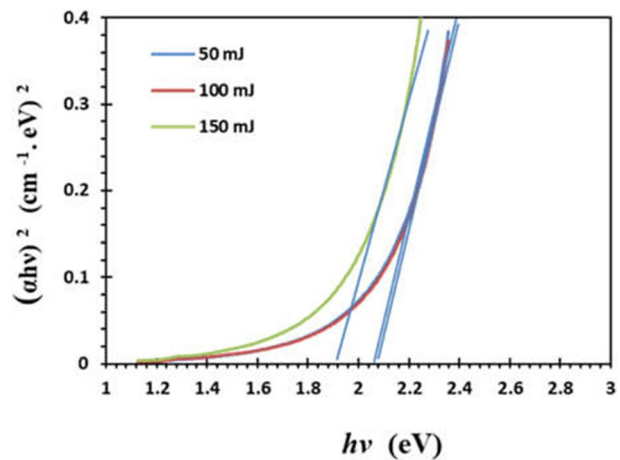
the optical absorption spectra of metal nanoparticles (Sarkar and Das 2018). The visible light absorption band is typical for Ag nanoparticles. The degree of nanoparticle aggregation influences the plasmon peak and full width at half maximum.

By increasing the pulse laser ablation energy from 50 to 150 mJ, we see a change in the SPR wavelength toward a more extended wavelength area (Fig. 4), indicative of a larger particle size. It is also clear from the absorption spectra that the peak broadens increases as the pulse laser intensity increases.

The plot of  $(\alpha h\nu)^2$  against  $h\nu$  for Ag@SiO<sub>2</sub> core-shell NPs can be seen in Fig. 5. In this figure,  $h$  represents Plank’s constant,  $\alpha$  represents the absorption coefficient, and  $\nu$  represents the frequency of the incident light. The energy gap of Ag@SiO<sub>2</sub> core-shell NPs has been determined by extending the linear section of  $(\alpha h\nu)^2$  to intersect with the  $h\nu$ -axis. When calculating the optical energy gap of the NPs, a well-known relation for direct transition is used (Salman and Ismail 2114).

$$\alpha h\nu = A(h\nu - E_g)^n \tag{4}$$

**Fig. 5** Optical energy bandgap for Ag@SiO<sub>2</sub> nanoparticles core-shell prepared at different laser energies



When  $A$  is a constant, the photon energy is denoted by  $h\nu$ , and  $n$  is  $\frac{1}{2}$  for the indirect and 2 for the direct band gap. The value of  $E_g$  was calculated using the extrapolation approach, and it was found to be 1.94, 2.06, and 2.08 eV for laser energies of 50 mJ, 100 mJ, and 150 mJ, respectively.

Time-resolved PL spectra and PL excitation measurements are also taken to analyze the PL spectra of Ag@SiO<sub>2</sub> core-shell better NPs. The excitation of electrons from occupied d bands into states above the Fermi level gives Ag its visible luminescence. An energy loss results from the Subsequencelectron-phenomenon and hole-phonon scattering, and then an electron from an occupied sp band combines with a hole to produce photoluminescence (Smitha et al. Nov. 2008).

Figure 6 depicts the luminescence spectra of the core-shell Ag@SiO<sub>2</sub> with various pulse laser energies. With increased laser energy, it has been seen that PL increases.

We use Planck's equation to determine the energy bandgap from the photoluminescence spectra of Ag@SiO<sub>2</sub> core-shell NPs.

$$E_g(eV) = \frac{1240}{\lambda(\text{nm})} \quad (5)$$

where  $E_g$  denotes the energy gap (eV), and the wavelength is characterized by  $\lambda$  (nm) in Eq. (5). The comparison between energy gap values calculated from UV-vis and PL measurements was tabulated in Table 3. The optical power gap computed from the two measures is close in value.

Figure 7 shows the TEM image Ag@SiO<sub>2</sub> prepared with laser ablation with (100.000 kX) magnification; the laser beam's energy is varied from 50 to 150 mJ, and the water thickness above the silver target is (0.8 cm). The image shows that Ag@SiO<sub>2</sub> core-shell nanoparticles form a sphere, and the size distribution of these particles can be seen in the size distribution chart.

As shown in Fig. 8, when the pulse laser energy was raised from 50 to 100 mJ, the average particle size rose significantly more than when the laser energy was increased from 100

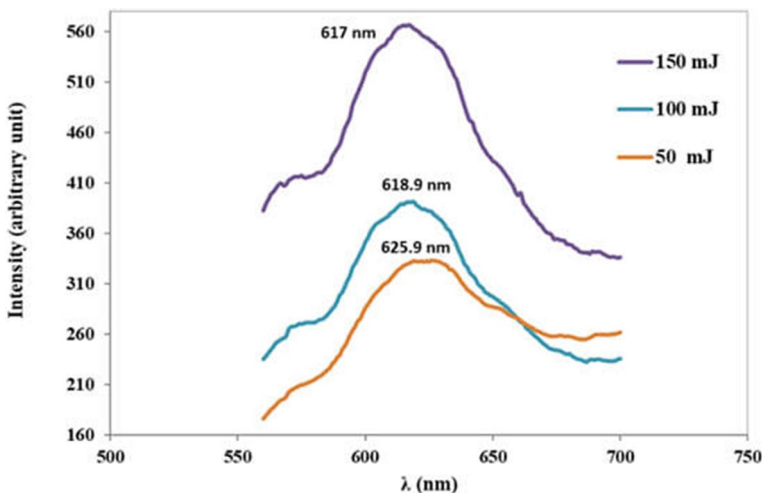


**Fig. 6** The photoluminescence (PL) spectra of Ag@SiO<sub>2</sub> core-shell NPs at various laser powers

**Table 3** Summarizes the results of the energy gap values estimated from the UV–Vis and PL measurements

Laser energy (mJ)	Eg, from UV–Vis (eV)	Eg, from PL (eV)
50	2.06	1.98
100	2.08	2
150	1.94	2

to 150 mJ. The transmission electron micrograph (TEM) picture of several Ag@SiO<sub>2</sub> can be shown in Fig. 9. The 5 nm SiO<sub>2</sub> shell is clearly seen around the silver NP core in this image.

Successful fabrication of a plasmonic dye-sensitized solar cell using TiO<sub>2</sub> paste. Two types of DSSC cells were prepared: regular DSSC and Plasmonic DSSC. The current density–voltage (J–V) characteristics of the DSSC under (AM1) illumination exhibited improved J<sub>sc</sub> and V<sub>oc</sub> for plasmonic cells compared with conventional cells and the power as a function of voltage as shown in Fig. 10a, b. The efficiency of DSSC has enhanced from (0.18%) to (0.23%) as a direct result of the utilization Ag@SiO<sub>2</sub>. Figure 10 present the J–V plot of regular DSSC and Plasmonic DSSC; the figure shows an increase in current density after adding Ag@SiO<sub>2</sub> core–shell nanoparticles.

Current–Voltage (I–V) measurements of a standard DSSC and a Plasmonic DSSC were performed in the dark, and under 100 mW/cm<sup>2</sup> of light were done To Investigate the mechanisms of current transport and photoconduction. The I–V graphs of the regular and Plasmonic DSSCs are shown in Fig. 11a–c. The relationship between current and voltage based on thermionic emission (TE) theory ( $V = 3kT/q$ ) can be studied using Eqs. (6) and (7).

$$I = I_o \left[ \exp\left(\frac{q(V - IR_s)}{nKT}\right) - 1 \right] \quad (6)$$

where n is the ideality factor, V is the applied voltage, k is the Boltzmann constant, T is the temperature in Kelvin, R<sub>s</sub> is the series resistance, and I<sub>o</sub> is the reverse-saturation current. At room temperature and above, Eq. (6) can be adjusted as follows since the value of R<sub>s</sub> can be ignored at low and moderate forward bias voltages.

$$\ln(I) = \ln(I_o) + \frac{qV}{nKT} \quad (7)$$

The slope and intercept of the ln(I)–V plot at zero bias was used to determine n and I<sub>o</sub>.

As can be seen from Fig. 10a–d, the value of the forwarding bias current does not change with increasing illumination intensity, but the reverse bias current increases because, in this region, both the inner and external electric fields have some direction. This increase in reverse current results from generated electron–hole pairs under illumination affected and named photocurrent (I<sub>ph</sub>). In other words, the photogenerated electron–hole pairs caused photoconductive behavior at the reverse bias zone (Altundal et al. 2022; Demirezen et al. 2021; Salman et al. 2019). The enhancement in DSSC's efficiency was basically related to photon absorbing efficiency of plasmonic Ag@SiO<sub>2</sub> NPs via the collective oscillations of surface electrons, which can be excited and directly injected into the conduction band of Titanium dioxide. Furthermore, the poor light absorption capability of TiO<sub>2</sub> can also be extended through the enhancement of the photoabsorption cross-section of dye molecules.



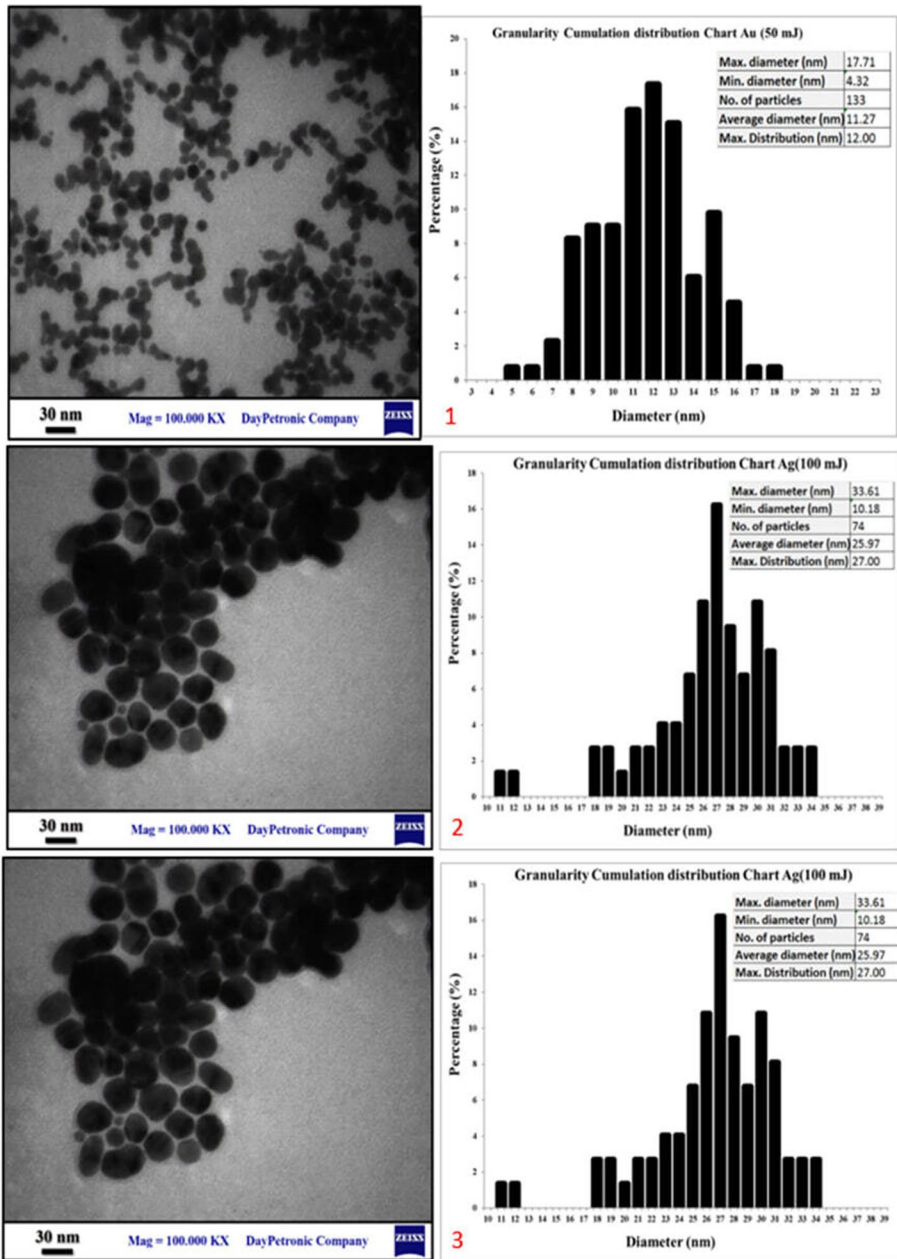
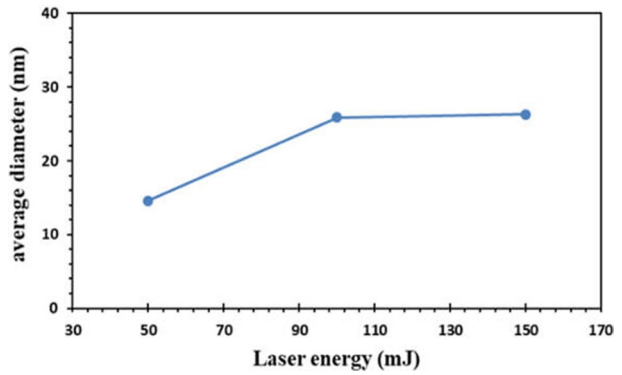


Fig. 7 Transmission electron micrograph (TEM) picture and size distribution chart of laser-ablated Ag@SiO<sub>2</sub> core-shell NPs generated at 1 50 mJ, 2 100 mJ, and 3 150 mJ

The efficiency of the solar cell is low compared to the results of other researchers. This is due to the fact that we used a small thickness of titanite as a photoanode. The reason for choosing the small thickness is to know the effect of adding Ag@SiO<sub>2</sub> NPs (Table 4).

**Fig. 8** Average diameter against laser energy



**Fig. 9** TEM picture of Ag@SiO<sub>2</sub>, which distinctly shows the presence of SiO<sub>2</sub> Nano shell

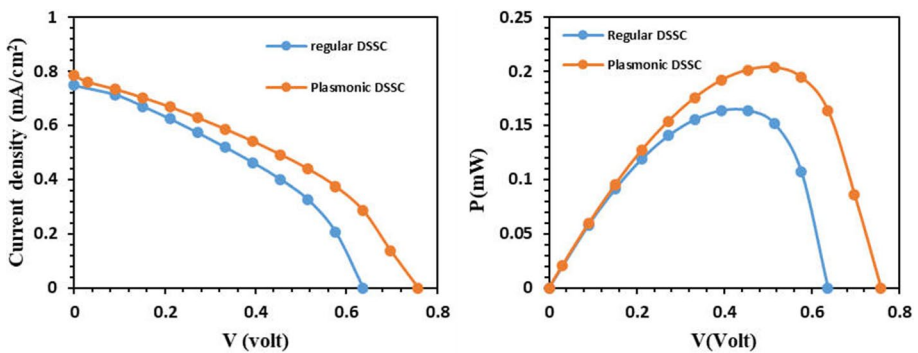
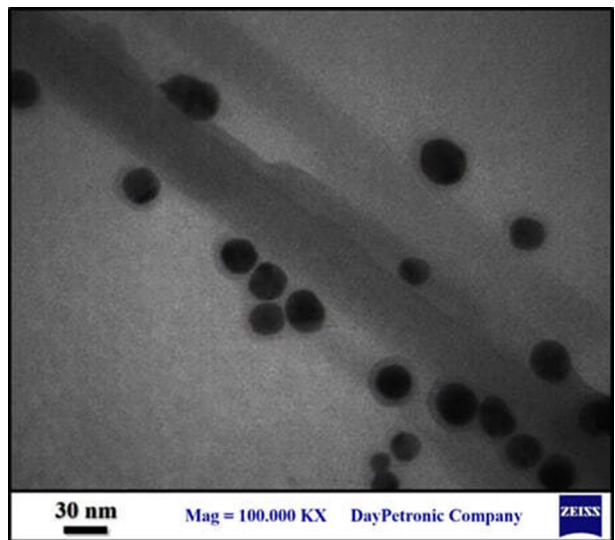


**Fig. 10** a J–V graphs of regular and Plasmonic DSSC under 100 mW/cm<sup>2</sup> at ambient temperature b power as a function of voltage

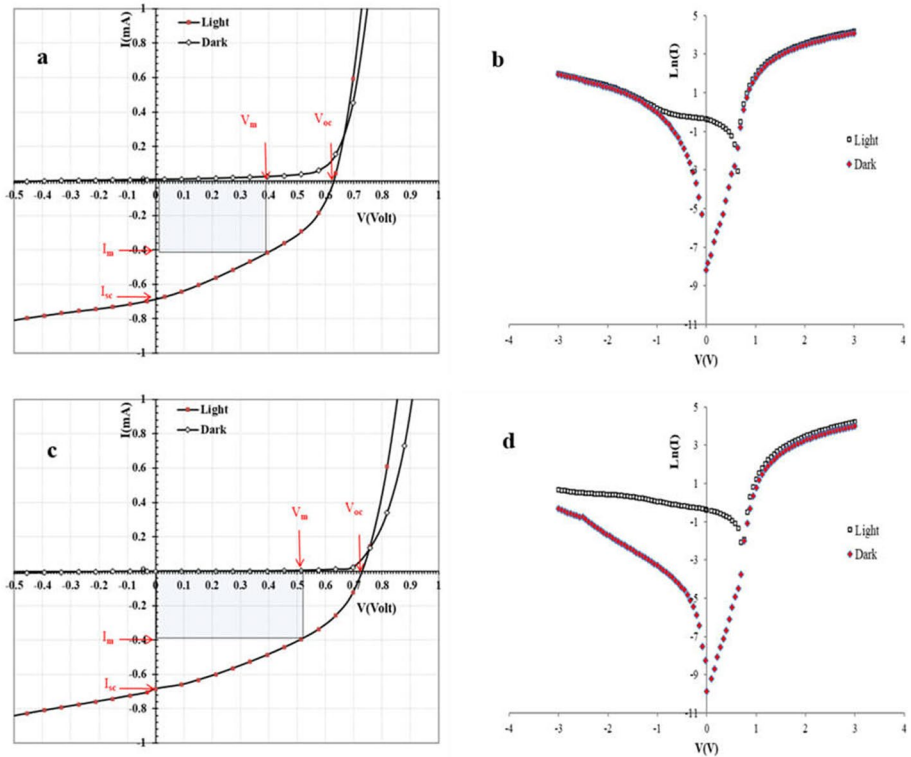


**Fig. 11** The I–V plot of **a, b** regular DSSC, **c, d** plasmonic DSSC with power lighting 100 mW/cm<sup>2</sup> and normal Room temperature

**Table 4** Summarizes the results of I–V measurements of regular and plasmonic DSSC

Solar cell type	$I_{sc}$ (mA)	$V_{oc}$ (V)	$I_m$ (mA)	$V_m$ (v)	FF	$\eta$ %	$R_{sh}$ ( $\Omega$ )	$R_s$ ( $\Omega$ )	n
Regular DSSC	0.68	0.63	0.42	0.39	0.39	0.18	2454.0	187.0	3.64
Plasmonic DSSC	0.70	0.74	0.39	0.52	0.39	0.23	2834.9	197.4	2.87

## 4 Conclusion

This research effectively synthesized Ag@SiO<sub>2</sub> core-shell NPs using laser ablation. The effect of energy on the structure of pulsed laser, optical, and morphological features of these nanoparticles was examined, as it was observed that the average particle size and crystallite size increased from 18.8 to 35 nm when laser energy was raised from 50 to 150 mJ. UV–Vis spectroscopy and photoluminescence results were consistent with each other for the optical energy gap. After increasing the laser ablation energy, a red shift in the surface plasmon resonance of Ag@SiO<sub>2</sub> Core-shell NPs from 398 to 402 nm indicating an increase in particle size. Ag@SiO<sub>2</sub> Core-shell nanoparticles were employed in manufactured solar dye-sensitized cells by taking advantage of the plasmon effect from these NPs

on the DSSCs efficiency, as it was observed that plasmonic-sensitized solar cell efficiency increased by 27% in comparison to the regular DSSC.

**Author contributions** Mohammed Adil Mohammed and Odai N. Salman did the experiments, gathered the data, and wrote the whole manuscript. MEHMET MAHİR BÜLBÜL contributed to analyzing the whole analysis used references to support claims, and also helped with experimental parts. All authors reviewed the manuscript.

**Funding** The authors have not disclosed any funding.

## Declarations

**Conflict of interest** The authors declared no conflict of interest.

## References

- Agrawal, A., Siddiqui, S.A., Soni, A., Sharma, G.D.: Advancements, frontiers and analysis of metal oxide semiconductor, dye, electrolyte and counter electrode of dye sensitized solar cell. *Sol. Energy* **233**, 378–407 (2022)
- Akram, M., Javed, H.M.A., Ghaffar, A., Majeed, M.I.: Investigations of Zr/TiO<sub>2</sub>-based nanocomposites for efficient plasmonic dye-sensitized solar cells. *Int. J. Mod. Phys. B* **37**(05), 2350042 (2023)
- Ali, A.K., Erten-Ela, S., Hassoon, K.I., Ela, Ç.: Plasmonic enhancement as selective scattering of gold nanoparticles based dye sensitized solar cells. *Thin Solid Films* **671**, 127–132 (2019). <https://doi.org/10.1016/j.tsf.2018.12.033>
- Alkhalayfeh, M.A., Aziz, A.A., Pakhuruddin, M.Z.: An overview of enhanced polymer solar cells with embedded plasmonic nanoparticles. *Renew. Sustain. Energy Rev.* **141**, 110726 (2021)
- Alkuam, E., Badrudeen, E., Guisbiers, G.: Influence of CdS morphology on the efficiency of dye-sensitized solar cells. *ACS Omega* **3**(10), 13433–13441 (2018). <https://doi.org/10.1021/acsomega.8b01631>
- Altındal, Ş., Azizian-Kalandaragh, Y., Ulusoy, M., Pirgholi-Givi, G.: The illumination effects on the current conduction mechanisms of the Au/(Er2O3:PVC)/n-Si (MPS) Schottky diodes. *J. Appl. Polym. Sci.* (2022). <https://doi.org/10.1002/app.52497>
- Arinze, E.S., Qiu, B., Nyirjesy, G., Thon, S.M.: Plasmonic nanoparticle enhancement of solution-processed solar cells: practical limits and opportunities. *ACS Photonics* **3**(2), 158–173 (2016). <https://doi.org/10.1021/acsp Photonics.5b00428>
- Arka, G.N., Prasad, S.B., Singh, S.: Comprehensive study on dye sensitized solar cell in subsystem level to excel performance potential: a review. *Sol. Energy* **226**, 192–213 (2021)
- Baby, R., Nixon, P.D., Kumar, N.M., Subathra, M.S.P., Ananthi, N.: A comprehensive review of dye-sensitized solar cell optimal fabrication conditions, natural dye selection, and application-based future perspectives. *Environ. Sci. Pollut. Res.* **29**, 1–34 (2022)
- Bao, Z., Fu, N., Qin, Y., Lv, J., Wang, Y., He, J., Hou, Y., Jiao, C., Chen, D., Wu, Y., Dai, J.: Broadband plasmonic enhancement of high-efficiency dye-sensitized solar cells by incorporating Au@ Ag@ SiO<sub>2</sub> core-shell nanocuboids. *ACS Appl. Mater. Interfaces* **12**(1), 538–545 (2019)
- Bhojanaa, K.B., Mohammed, J.J., Manishvarun, M., Pandikumar, A.: Dye-sensitized solar cells with efficiency enhancement surpassing 65% through layer-by-layer assembled plasmonic photoanodes. *J. Power. Sources* **558**, 232593 (2023)
- Bi, W., Wu, Y., Chen, C., Zhou, D., Song, Z., Li, D., Chen, G., Dai, Q., Zhu, Y., Song, H.: Dye sensitization and local surface plasmon resonance-enhanced upconversion luminescence for efficient perovskite solar cells. *ACS Appl. Mater. Interfaces* **12**(22), 24737–24746 (2020)
- Choudhury, B.D.: Flexible dye-sensitized solar cells: a study of photoanode and counter electrode materials. Doctoral dissertation, The University of Texas Rio Grande Valley (2020)
- Demirezen, S., Çetinkaya, H.G., Kara, M., Yakuphanoglu, F., Altındal, S.: Synthesis, electrical and photosensing characteristics of the Al/(PCBM/NiO: ZnO)/p-Si nanocomposite structures. *Sens. Actuators A Phys.* (2021). <https://doi.org/10.1016/j.sna.2020.112449>
- Di, Y., Qin, T.: Plasmonic ZrN@ TiO<sub>2</sub> core-shell nanostructure enhancing photovoltaic performance of dye-sensitized solar cells. *Opt. Mater.* **132**, 112813 (2022)

- Dragonetti, C., Magni, M., Colombo, A., Melchiorre, F., Biagini, P., Roberto, D.: Coupling of a copper dye with a copper electrolyte: a fascinating springboard for sustainable dye-sensitized solar cells. *ACS Appl. Mater. Interfaces* **1**(2), 751–756 (2018). <https://doi.org/10.1021/acsaem.7b00196>
- Drexhage, K.H.: Influence of a dielectric interface on fluorescence decay time (1970)
- Eicke, L., Eicke, A., Hafner, M.: Solar power generation. In: Hafner, M., Luciani, G. (eds.) *The palgrave handbook of international energy economics*. Palgrave Macmillan, Cham (2022). [https://doi.org/10.1007/978-3-030-86884-0\\_9](https://doi.org/10.1007/978-3-030-86884-0_9)
- Fallah, M., Maleki, I., Zamani-Meymian, M.R., Abdi, Y.: Enhancing the efficiency of dye-sensitized solar cell by increasing the light trapping and decreasing the electron-hole recombination rate due to Ag@ TiO<sub>2</sub> core-shell photoanode structure. *Mater. Res. Express* **7**(1), 016409 (2019)
- Furugori, S., Kobayashi, A., Watanabe, A., Yoshida, M., Kato, M.: Impact of photosensitizing multilayered structure on ruthenium(II)-dye-sensitized TiO<sub>2</sub>-nanoparticle photocatalysts. *ACS Omega* **2**(7), 3901–3912 (2017). <https://doi.org/10.1021/acsomega.7b00566>
- Guo, M., Chen, J., Zhang, J., Su, H., Liu, L., Fu, N., Xie, K.: Coupling plasmonic nanoparticles with TiO<sub>2</sub> nanotube photonic crystals for enhanced dye-sensitized solar cells performance. *Electrochim. Acta* **263**, 373–381 (2018)
- He, X., Guo, Y., Li, X., Liu, J.: In situ ligand-free growth of TiO<sub>2</sub>-encapsulated Au nanocomposites on photoanode for efficient dye sensitized solar cells. *Chem. Eng. J.* (2020). <https://doi.org/10.1016/j.cej.2020.125302>
- Huang, Y., Wu, H., Yu, Q., Wang, J., Yu, C., Wang, J., Gao, S., Jiao, S., Zhang, X., Wang, P.: Single-layer TiO<sub>2</sub> film composed of mesoporous spheres for high-efficiency and stable dye-sensitized solar cells. *ACS Sustain. Chem. Eng.* **6**(3), 3411–3418 (2018)
- Juma, M.W., Nancy, M.M., Birech, Z., Ondieki, A.M., Maaza, M., Mkhochtwa, D.: Using laser ablation in liquid (LASIS) method to synthesize silver nanoparticles for SERS applications. *Mater. Today Proc.* (2023)
- Kaimuangpak, K., Tamprasit, K., Date, A., Wongwiwatthanakit, S., Chang, L.C., Weerapreeyakul, N.: Synthesis of bioactive spherical silver nanoparticles with surface plasmon resonance using ethanolic twig extract of *Cratogeomys formosus* ssp. *pruniflorum*. *J. Drug Deliv. Sci. Technol.* **88**, 104897 (2023)
- Kankanamge, H.K.H.D., Kumari, J.M.K.W., Dissanayake, M.A.K.L., Senadeera, G.K.R., Dassanayake, B.S., Perera, H.C.S.: Highly efficient dye-sensitized solar cells with TiO<sub>2</sub>-coated silver nanowire-incorporated tri-layered photoanode. *Bull. Mater. Sci.* **46**(3), 145 (2023)
- Maka, A.O., Alabid, J.M.: Solar energy technology and its roles in sustainable development. *Clean Energy* **6**(3), 476–483 (2022)
- Mandal, P.: Application of plasmonics in solar cell efficiency improvement: a brief review on recent progress. *Plasmonics* **17**(3), 1247–1267 (2022)
- Mehmood, U., Ahmed, S., Hussein, I.A., Harrabi, K.: Improving the efficiency of dye sensitized solar cells by TiO<sub>2</sub>-graphene nanocomposite photoanode. *Photonics Nanostruct.* **16**, 34–42 (2015). <https://doi.org/10.1016/j.photonics.2015.08.003>
- Noorasad, N.S., Arith, F., Mustafa, A.N., Azam, M.A., Mahalingam, S., Chelvanathan, P., Amin, N.: Current advancement of flexible dye sensitized solar cell: a review. *Optik* **254**, 168089 (2022)
- O'Regan, B., Grätzel, M.: A low-cost, high-efficiency solar cell based on dye-sensitized colloidal TiO<sub>2</sub> films. *Nature* **353**, 737–740 (1991). <https://doi.org/10.1038/353737a0>
- Park, J.H., Kim, U.Y., Kim, B.M., Kim, W.H., Roh, D.H., Kim, J.S., Kwon, T.H.: Molecular design strategy toward robust organic dyes in thin-film photoanodes. *ACS Appl. Energy Mater.* **2**(7), 4674–4682 (2019)
- Rahman, S., Haleem, A., Siddiq, M., Hussain, M.K., Qamar, S., Hameed, S., Waris, M.: Research on dye sensitized solar cells: recent advancement toward the various constituents of dye sensitized solar cells for efficiency enhancement and future prospects. *RSC Adv.* **13**(28), 19508–19529 (2023)
- Rai, P.: Plasmonic noble metal@metal oxide core-shell nanoparticles for dye-sensitized solar cell applications. *Sustain. Energy Fuels* **3**, 63–91 (2019). <https://doi.org/10.1039/C8SE00336j>
- Rho, W.Y., Yang, H.Y., Kim, H.S., Son, B.S., Suh, J.S., Jun, B.H.: Recent advances in plasmonic dye-sensitized solar cells. *J. Solid State Chem.* **258**, 271–282 (2018)
- Rong, P., Ren, S., Yu, Q.: Fabrications and applications of ZnO nanomaterials in flexible functional devices—a review. *Crit. Rev. Anal. Chem.* **49**(4), 336–349 (2019)
- Salimi, K., Atilgan, A., Aydin, M.Y., Yildirim, H., Celebi, N., Yildiz, A.: Plasmonic mesoporous core-shell Ag-Au@ TiO<sub>2</sub> photoanodes for efficient light harvesting in dye sensitized solar cells. *Sol. Energy* **193**, 820–827 (2019)
- Salman, O.N., Ahmed, D.S., Abed, A.L., Dawood, M.O.: Preparation pure ZnO, La-doped ZnO nanoparticles using sol-gel technique: characterization and evaluation antibacterial activity. In: *IOP*

- Conference Series: Materials Science and Engineering, Institute of Physics Publishing (2019). <https://doi.org/10.1088/1757-899X/518/3/032012>
- Salman, O.N., Ismail, M.M., Ali, T.H.: Growth time influence on optical and electrical properties of TiO<sub>2</sub> nanorods prepared via hydrothermal method. *J. Phys. Conf. Ser.* **2114**, 012063 (2021). <https://doi.org/10.1088/1742-6596/2114/1/012063>
- Salman, O.N., Ismail, M.M., Dawood, M.O.: Porous BaTiO<sub>3</sub> film for dye-sensitized solar cells. *Opt. Quant. Electron.* **55**, 469 (2023). <https://doi.org/10.1007/s11082-023-04741-9>
- Sampaio, R.N., Müller, A.V., Polo, A.S., Meyer, G.J.: Correlation between charge recombination and lateral hole-hopping kinetics in a series of cis-Ru(phen')(dcb)(NCS)<sub>2</sub> dye-sensitized solar cells. *ACS Appl. Mater. Interfaces* **9**(39), 33446–33454 (2017). <https://doi.org/10.1021/acsami.7b01542>
- Sarkar, S., Das, R.: Determination of structural elements of synthesized silver nano-hexagon from X-ray diffraction analysis. *Indian J. Pure Appl. Phys.* **56**, 765–772 (2018)
- Selvapriya, R., Abhijith, T., Ragavendran, V., Sasirekha, V., Reddy, V.S., Pearce, J.M., Mayandi, J.: Impact of coupled plasmonic effect with multishaped silver nanoparticles on efficiency of dye sensitized solar cells. *J. Alloy. Compd.* **894**, 162339 (2022)
- Septiningrum, F., Sofyan, N., Dhaneswara, D., Reddy, M.V., Yuwono, A.H.: One-dimensional silver-titania nanocomposites as modification of photoanode for enhanced dye-sensitized solar cells—a review. *Mater. Today Proc.* **62**, 3301–3305 (2022)
- Smitha, S.L., Nissamudeen, K.M., Philip, D., Gopchandran, K.G.: Studies on surface plasmon resonance and photoluminescence of silver nanoparticles. *Spectrochim. Acta A Mol. Biomol. Spectrosc.* **71**(1), 186–190 (2008). <https://doi.org/10.1016/j.saa.2007.12.002>
- Villanueva-Cab, J., Olalde-Velasco, P., Romero-Contreras, A., Zhuo, Z., Pan, F., Rodil, S.E., Yang, W., Pal, U.: Photocharging and band gap narrowing effects on the performance of plasmonic photoelectrodes in dye-sensitized solar cells. *ACS Appl. Mater. Interfaces* **10**(37), 31374–31383 (2018)
- Yang, H., Yang, B., Chen, W., Yang, J.: Preparation and photocatalytic activities of TiO<sub>2</sub>-based composite catalysts. *Catalysts* **12**(10), 1263 (2022)
- Yen, Y.C., Chen, J.A., Ou, S., Chen, Y.S., Lin, K.J.: Plasmon-enhanced photocurrent using gold nanoparticles on a three-dimensional TiO<sub>2</sub> nanowire-web electrode. *Sci. Rep.* (2017). <https://doi.org/10.1038/srep42524>
- Zhang, P., Hu, Z., Wang, Y., Qin, Y., Li, W., Wang, J.: A Bi-layer composite film based on TiO<sub>2</sub> hollow spheres, P25, and multi-walled carbon nanotubes for efficient photoanode of dye-sensitized solar cell. *Nanomicro Lett.* **8**(3), 232–239 (2016). <https://doi.org/10.1007/s40820-015-0081-1>

**Publisher's Note** Springer Nature remains neutral with regard to jurisdictional claims in published maps and institutional affiliations.

Springer Nature or its licensor (e.g. a society or other partner) holds exclusive rights to this article under a publishing agreement with the author(s) or other rightsholder(s); author self-archiving of the accepted manuscript version of this article is solely governed by the terms of such publishing agreement and applicable law.